

Accepted Manuscript

“Half-sandwich” Schiff-base Ir(III) complexes as anticancer agents

Ze-dong Mou, Ning Deng, Feng Zhang, Jiaying Zhang, Juan Cen, Xia Zhang



PII: S0223-5234(17)30473-7

DOI: [10.1016/j.ejmech.2017.06.027](https://doi.org/10.1016/j.ejmech.2017.06.027)

Reference: EJMECH 9522

To appear in: *European Journal of Medicinal Chemistry*

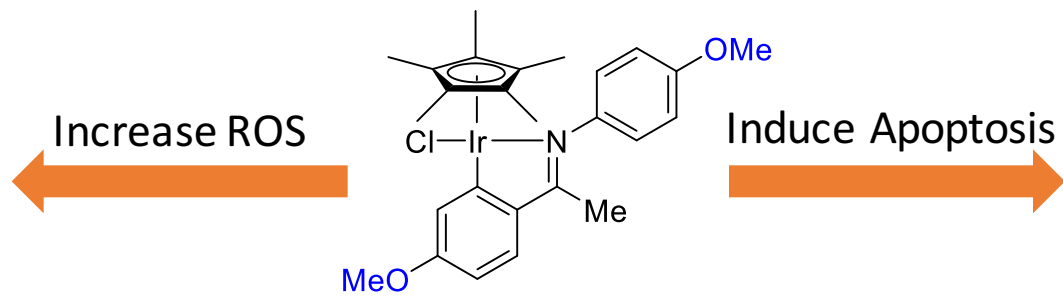
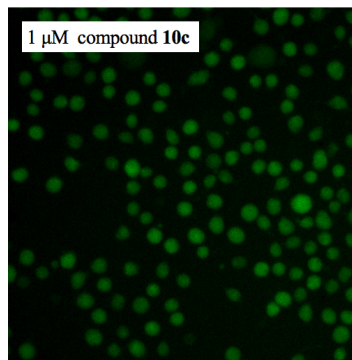
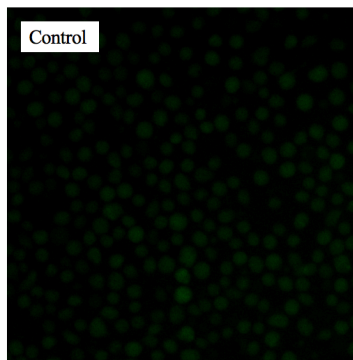
Received Date: 17 March 2017

Revised Date: 13 June 2017

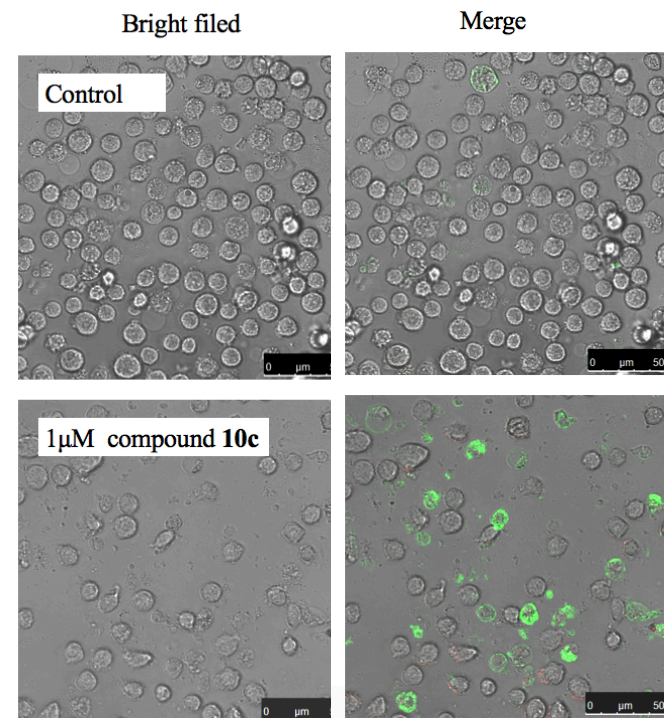
Accepted Date: 14 June 2017

Please cite this article as: Z.-d. Mou, N. Deng, F. Zhang, J. Zhang, J. Cen, X. Zhang, “Half-sandwich” Schiff-base Ir(III) complexes as anticancer agents, *European Journal of Medicinal Chemistry* (2017), doi: 10.1016/j.ejmech.2017.06.027.

This is a PDF file of an unedited manuscript that has been accepted for publication. As a service to our customers we are providing this early version of the manuscript. The manuscript will undergo copyediting, typesetting, and review of the resulting proof before it is published in its final form. Please note that during the production process errors may be discovered which could affect the content, and all legal disclaimers that apply to the journal pertain.



IC₅₀ (K562) = 0.26 μM
IC₅₀ (K562/A02) = 1.95 μM



“Half-sandwich” Schiff-base Ir(III) complexes as anticancer agents

Ze-dong Mou^{a,†}, Ning Deng^{a,†}, Feng Zhang^b, Jiaying Zhang^a, Juan Cen^{b,*}, and Xia Zhang^{a,*}

^a State Key Laboratory of Biotherapy and Department of Ophthalmology, West China Hospital, Sichuan University and Collaborative Innovation Center, Chengdu 610041, China

^b Key Laboratory of Natural Medicine and Immune Engineering, Henan University, Kaifeng 475004, China

* Corresponding authors. E-mail addresses: cenjuan@henu.edu.cn (J. C.), zhang-xia@scu.edu.cn (X. Z.).

Tel./fax: +86 378 2864665(J. C.), +86 28 85503817 (X. Z.).

[†] These authors contributed equally.

Abstract

A series of “half-sandwich” Schiff-base Ir(III) complexes were synthesized and investigated for their *in vitro* activities against the leukemia K562 cell line. These compounds demonstrated antiproliferative activities against K562 cells with IC₅₀ values of 0.26 - 4.77 μ M. In particular, compound **10c** showed cytotoxicity against five cancer cell lines/sublines and stronger activities than cisplatin in K562, K562/A02, MCF-7, MCF-7/ADM, and A549 cells. Mechanism studies illustrated that compound **10c** increased the level of reactive oxygen species and induced apoptosis of K562 cells. This compound effectively decreased the mitochondrial membrane potential and the protein level of Bcl-2. It also increased the protein levels of Bax, caspase-3, and caspase-9, and led to release of cytochrome c in K562 cells, indicating that the apoptosis induced by compound **10c** was mediated by the intrinsic mitochondria apoptosis pathway.

Key Words: Schiff-base Ir(III) complexes; antiproliferative activities; reactive oxygen species; apoptosis.

1. Introduction

Because of their variations in coordination numbers, geometries, and properties of the metal ion and ligands, transition metals provide highly versatile scaffolds for drug design. [1-3] Not surprisingly, the discovery of cisplatin and the other two platinum-based drugs, carboplatin and oxaliplatin, represented the most successful examples in the field of medicinal inorganic chemistry. Cisplatin and its analogues function as anticancer drugs mainly by forming platinum-DNA adducts that interfere with DNA replication and further lead to cell death.[4, 5] Although these platinum-based drugs are among the most widely used anticancer therapeutics, they produce undesirable side effects and easily acquired drug resistance.[6, 7] The success and limitations of these platinum-based drugs stimulated tremendous research efforts into the discovery of other transition metal-based anticancer drugs. It is expected that transition metal-based anticancer drugs with mechanisms of action different from those of the platinum-based drugs would demonstrate diminished side effects, no easily developed drug resistance, and/or a broader spectrum of anticancer activities.[8, 9]

Recently, in addition to other transition metal complexes including Ru-, Rh-, Re-, Os-, and Au-based compounds, anticancer Ir(III) complexes received significant attentions.[1, 2, 9-11] Interestingly, complexes of Ir(III), a third-row low-spin d^6 metal ion, were initially considered to be too inert to exhibit high anticancer activities.[12] This is probably because that hydrolysis is usually an key step in the mechanism of action of metal-based anticancer agents, and yet the process of exchanging an aqua ligand on $[\text{Ir}(\text{H}_2\text{O})_6]^{3+}$ takes hundreds of years.[13-15] In fact, an Ir analogue of NAMI-A (a Ru-based antitumor metastasis agent on clinical trials), trans- $[\text{IrCl}_4(\text{DMSO})(\text{Im})][\text{ImH}]$ (DMSO = dimethyl sulfoxide, ImH = imidazole), was kinetically inert towards hydrolysis and was also biologically inactive.[16] However, Meggers and co-workers took advantage of the kinetic inertness and structural opportunities provided by the octahedral geometries of Ir(III), and successfully designed a selective Ir(III)-based inhibitor of the receptor tyrosine kinase FLT4 (also known as VEGFR3) as anticancer agents (compound **1** in Figure 1).[17, 18] The Sadler group and the Sheldrick group found that the anticancer activities of Ir(III) complexes strongly depended on their ligand sets.[19] For instance, the “half-sandwich” pentamethylcyclopentadienyl (Cp^*) iridium(III) complex **2** was biologically inactive, while by the incorporation of phenyl substituents as in phenyltetramethylcyclopentadienyl (Cp^{xph}) and biphenyltetramethylcyclopentadienyl (Cp^{xbiph}) ligands, iridium(III) complexes **3** and **4** both

demonstrated activities against A2780 cancer cells.[14] The introduction of the C,N-chelating ligands instead of the N,N-chelating ligands also improved the antiproliferative activities of the iridium(III) complexes (see compounds **5** and **6** in Figure 1).[20] In addition, Ma and other groups identified several series of cyclometalated Ir(III) complexes with favorable anticancer activities.[21-25] However, to date, no Ir(III) complex has reached the market. Efforts are still needed to discover novel Ir(III) complexes that will benefit the cancer patients.

Our group was previously inspired by the special characteristics of the iridium complexes as catalysts and developed iridium-based asymmetric synthetic methodologies.[26, 27] The recently reported anticancer activities of Ir(III)-based compounds intrigued our interest in exploring the functions of Ir(III) complexes in biological systems. In order to identify novel Ir(III)-based anticancer agents, we synthesized a series of “half-sandwich” Schiff-base Ir(III) complexes. We report herein the anticancer activities, the structure-activity relationship analysis, and the preliminary mechanism studies of these compounds.

2. Results and discussion

2.1 Chemistry

The general synthetic route for the targeted “half-sandwich” Schiff-base Ir(III) complexes **10a-o** is outlined in Scheme 1.[28, 29] The easily accessible ketones **7** was treated with anilines **8** to obtain the ketimines **9**. Then, the reaction of 1.0 equivalent of $[\text{Cp}^*\text{IrCl}_2]_2$ with 2.0 equivalents of ketimine **9** in the presence of 10.0 equivalents of NaOAc in dichloromethane (DCM) for 24 h afforded the Ir(III) complexes in moderate to high yields. All new complexes were characterized by ^1H NMR, ^{13}C NMR, IR, and ESI-MS analysis.

2.2. Biological evaluation

2.2.1. *In vitro* antiproliferative activity and structure-activity relationship analysis

The *in vitro* antiproliferative activities of the compounds **10a-o** were evaluated against the leukemia K562 cell line and the corresponding IC_{50} (the concentration leading to 50% inhibition of the cancer cell proliferation) values were listed in Table 1. Complexes **10a-o** demonstrated promising antiproliferative activities against K562 cells, and all showed higher potency than cisplatin. Although the antiproliferative activities of these compounds fell within a relatively narrow range (from 0.26 μM to 4.77 μM), the differences illustrated the effects of the

Schiff-base ligands of these Ir(III) complexes on their activities in the K562 cells. In most cases, compounds containing electron-donating groups showed better potency than their counterparts without electron-donating groups. The complex **10k** with a strong electron-withdrawing nitro group showed the worst activity ($IC_{50} = 4.77 \mu M$), while compound **10c** containing two electron-donating methoxy groups demonstrated the highest potency ($IC_{50} = 0.26 \mu M$). Further analysis revealed that electron-donating groups on the para-position of ring A favorably contributed to the activity of the compounds and electron-withdrawing groups led to decrease of the activity of the complexes (compounds **10j** vs. **10e**, **10i** vs. **10h** and **10g**, and **10d** vs. **10k**, **10l**, and **10n**). This probably is because hydrolysis is a key step in the mechanism of action as mentioned above and the electron-donating groups facilitate the leaving of the chloride ions, accelerating the hydrolysis. Substituents on ring B might affect the activity of the compounds through a combination of electrostatic and other effects. For instance, in cases of compounds **10a**, **10c**, and **10d**, compounds **10h** and **10k**, or compounds **10f** and **10g**, electrostatic effects dominantly affected the activities of these compounds, where electron-donating groups on ring B resulted in increase of the activities of the compounds and electron-withdrawing group led to decrease of the activity of the complexes. In cases of compounds **10b** and **10d**, or compounds **10e** and **10f**, the potency of complexes with no substituents on the phenyl ring was slightly lower than those with electron-withdrawing chloro or trifluoromethyl substituents. This may indicate the specific requirements of these complexes to interact with its targets in cells.

The activities of compound **10c** (the most active in K562 cells) against a series of other cancer cell lines/sublines including K562/A02, MCF-7, MCF-7/ADM, and A549 cells were further investigated (Table 2). In all cancer cells tested, compound **10c** displayed stronger potency than cisplatin. Because of the strong activities of compound **10c** in multiple cell lines, the mechanisms of its antiproliferative effects were further investigated.

2.2.2. ROS assessment

The effect of compound **10c** on the level of intracellular ROS (iROS) in K562 cells was measured using the DCFH-DA method. The treatment with compound **10c** as well as the treatment with cisplatin both increased the levels of iROS compared with the untreated control cells (Figure 2). In addition, the ROS scavenger N-acetyl-L-cysteine (NAC) attenuated the iROS induced by compound **10c**.

2.2.3. Apoptosis assessment

The ability of compound **10c** to provoke apoptosis in K562 cells was then evaluated. As shown in Figure 3, the percentage of early apoptotic cells (Annexin V⁺/PI⁻) after the treatment with compound **10c** for 24 h increased from 0.9±0.5% (control) to 12.2±2.7%. NAC significantly restored the percentage of early apoptosis cells in the presence of 1 μM compound **10c**. This effect was consistent with the result of the ROS assay, suggesting that compound **10c** induced apoptosis in a ROS-dependent manner. In addition, the percentage of cells in late apoptosis or necrosis (annexin-V⁺/PI⁺) also increased after the treatment with compound **10c**, but without statistically significance compared with the effect caused by cisplatin.

2.2.4. The mitochondrial pathway of apoptosis induced by compound 10c

Our investigations then demonstrated that compound **10c** triggered the mitochondrial pathway of apoptosis. As shown in Figure 4, the intensity of green fluorescence (JC-1 monomers) was substantially increased in the presence of compound **10c** at 1 μM, indicating that compound **10c** led to a decrease in the mitochondrial membrane potential of K562 cells. The decrease of the mitochondrial membrane potential caused by compound **10c** was significantly reversed by NAC at 2 mM, demonstrating that the effect of compound **10c** on mitochondrial membrane potential was correlated with the ROS level in the cells. Figure 5A showed the concentration-dependent release of cytochrome c (an apoptogenic factor) into the cytosol in K562 cells treated with compound **10c**, suggesting that the induced apoptosis was likely to be mediated by the intrinsic mitochondria apoptosis pathway. Moreover, compound **10c** down-regulated the expression of Bcl-2 (an anti-apoptotic factor) and up-regulated Bax (a pro-apoptotic factor) in a dose-dependent manner. The reduction of the ratio of Bcl-2/Bax also indicated the activation of mitochondrial apoptotic pathway after the treatment with compound **10c**. We then analyzed the activity of caspase-9, a typical marker of mitochondrial apoptotic pathway. As shown in Figure 5B, compound **10c** significantly elevated the activities of caspase-9 and caspase-3. Caspase-9 was 1.20, 1.80, 2.48, and 2.68 times as active as the control and caspase-3 was 1.16, 1.65, 2.14, and 2.25 times as active as the control after the treatments with compound **10c** at 0.1, 0.3, 1, and 3 μM, respectively.

2.2.5. Cell cycle analysis

The effects of compound **10c** on cell cycle distribution were examined using flow cytometry. As shown in Figure 6, the treatment with 1 μ M compound **10c** for 48 h significantly enhanced sub diploid cells and decreased cells in S phase and G_0/G_1 phase. The results also demonstrated that cisplatin induced the accumulation of K562 cells in G_0/G_1 phase, indicating that compound **10c** had different mechanisms of action from cisplatin. The treatment with NAC partially reversed the effects of compound **10c**. In addition, the induction of cell death by the treatment with compound **10c** was also confirmed by the flow cytometric analysis of cell cycle.

3. Experimental Section

3.1. Synthesis

3.1.1. Materials and methods

^1H NMR and ^{13}C NMR spectra were recorded on a Bruker 400 MHz NMR spectrometer (Bruker AMX 400, Fällanden, Switzerland) at 400 and 100 MHz, respectively. Chemical shifts (δ) were reported in ppm with tetramethylsilane as the internal standard. IR spectra were recorded on a Thermo Scientific Nicolet iS5 spectrometer (iD5 ATR, diamond). ESI-HRMS spectra were recorded on a Waters SYNAPT G2. Melting points were recorded at SGW X-4 melting point instrument (Shanghai precision & scientific instrument Co., Ltd, Shanghai, China). All reagents and solvents were purchased from Admas, Aldrich, Energy Chemical, J&K, and Strem Chemicals, and used as received. Column chromatography was performed on silica gel (300-400 mesh, Qingdao Marine Chemical Ltd, Qingdao, China).

3.1.2. General procedures for the preparation of $[\text{Cp}^*\text{IrCl}_2]_2$

To a solution of $\text{IrCl}_3 \cdot 3\text{H}_2\text{O}$ (1.4950 g, 5.0 mmol) in 10 mL methanol was added pentamethylcyclopentadiene (1.0200 g, 7.5 mmol). The mixture was refluxed for 36 h. After the mixture was cooled to room temperature, the product $[\text{Cp}^*\text{IrCl}_2]_2$ was precipitated out, filtered, washed with cold methanol, dried under vacuum, and used without further purification.

3.1.3. General procedures for the preparation of ketimines

Under a N_2 atmosphere, dichloromethane (25 mL), Et_3N (20 mmol), ketone (10 mmol), and amine (12 mmol) were added into a round bottom flask. TiCl_4 (5 mmol) in dichloromethane

(10 mL) was added dropwise under N₂ at 0 °C within 15 min. The reaction mixture was stirred at 0 °C for 0.5 h, then warmed up to 25 °C and stirred at 25 °C for 7-8 h. The reaction mixture was quenched with a saturated solution of K₂CO₃ (30 mL), and the reaction mixture was filtered through a Buchner funnel. The organic layer was separated from the filtrate, and the remaining aqueous layer was extracted with dichloromethane (2×25 mL). The combined organic layer was washed with brine (10 mL) and dried over anhydrous Na₂SO₄. The solvent was removed under vacuum, and then the ketimine was recrystallized from ethanol.

3.1.4. General procedures for the preparation of the iridium complexes

[Cp*IrCl₂]₂ (1.0 equiv), ketimine (2.0 equiv), and NaOAc (10.0 equiv) were placed into a Schlenk tube. The tube was then transferred into a nitrogen-filled glove-box. Dichloromethane was then added and the resulting mixture was stirred at room temperature for 24 h. The reaction mixture was filtered through celite, and dried over Na₂SO₄. After removal of the solvent under vacuum the resulting solid was washed with diethyl ether/petroleum ether to afford the iridium complexes.

3.1.5. Analytical and spectral characterization data

[(η⁵-Cp*)Ir((E)-4-((1-(4-methoxyphenyl)ethylidene)amino)benzotrile)Cl] 10a:

Yellow solid (26.3 mg, 0.05 mmol, 86%); m.p. = 220 ~ 222 °C; ¹H NMR (400 MHz, CDCl₃, 298 K) δ (ppm): δ 7.93 (s, 1H), 7.74 (d, *J* = 7.4 Hz, 2H), 7.51 (d, *J* = 8.4 Hz, 1H), 7.35 (s, 1H), 6.96 (s, 1H), 6.61 (d, *J* = 8.4 Hz, 1H), 3.91 (s, 3H), 2.40 (s, 3H), 1.41 (s, 15H); ¹³C NMR (100 MHz, CDCl₃, 298 K) δ (ppm): 179.70, 170.89, 161.62, 153.47, 139.54, 129.88, 118.22, 117.49, 108.66, 107.41, 88.10, 54.08, 15.92, 7.54; IR (thin film, cm⁻¹): 2960, 2357, 1534, 1456, 1342, 1257, 1013, 791, and 748; HRMS (ESI) for C₂₆H₂₈ClIrN₂O [M-Cl]⁺: m/z calc.: 577.1831, Found: 577.1855.

[(η⁵-Cp*)Ir((E)-1-(4-methoxyphenyl)-N-(4-(trifluoromethyl)phenyl)ethan-1-imine)Cl] 10b:

Yellow solid (27.6 mg, 0.05 mmol, 84%); m.p. = 245 ~ 247 °C; ¹H NMR (400 MHz, CDCl₃, 298 K) δ (ppm): 8.19 – 7.81 (m, 1H), 7.70 (d, *J* = 8.3 Hz, 2H), 7.50 (d, *J* = 8.6 Hz, 1H), 7.36 (d, *J* = 2.5 Hz, 1H), 7.19 – 6.91 (m, 1H), 6.61 (dd, *J* = 8.6, 2.5 Hz, 1H), 3.92 (s, 3H), 2.41 (s, 3H), 1.42 (s, 15H); ¹³C NMR (100 MHz, CDCl₃, 298 K) δ (ppm): 180.51, 171.36, 162.40, 153.66, 140.71, 130.58, 128.08 (q, *J* = 23 Hz), 123.91 (q, *J* = 270 Hz), 119.18, 108.15, 89.01, 55.00, 16.83, 8.44;

IR (thin film, cm^{-1}): 2962, 2367, 1537, 1455, 1377, 1272, 1014, 795, and 749; HRMS (ESI) for $\text{C}_{26}\text{H}_{28}\text{ClIrNO}$ $[\text{M}-\text{Cl}]^+$: m/z calc.: 620.1752, Found: 620.1768.

$[(\eta^5\text{-Cp}^*)\text{Ir}(\text{E})\text{-N,1-bis(4-methoxyphenyl)ethan-1-imine)Cl]$ 10c:

Yellow solid (purchased from Strem Chemicals); the characterization data are as follows and consistent with the reported data.[30] ^1H NMR (400 MHz, CDCl_3 , 253 K) δ (ppm): 7.79 (d, $J = 8.8$ Hz, 1H), 7.72 (d, $J = 8.2$ Hz, 1H), 7.07 (d, $J = 2.5$ Hz, 1H), 7.02-6.95 (m, 2H), 6.91 (d, $J = 8.1$ Hz, 1H), 6.81 (d, $J = 8.3$ Hz, 1H), 3.88 (s, 3H), 3.83 (s, 3H), 2.44 (s, 3H), 1.44 (s, 15H); HRMS for $\text{C}_{26}\text{H}_{31}\text{ClIrNO}_2$ $[\text{M}-\text{Cl}]^+$: m/z calc.: 582.1984, Found: 582.1980.

$[(\eta^5\text{-Cp}^*)\text{Ir}(\text{E})\text{-1-(4-methoxyphenyl)-N-phenylethan-1-imine)Cl]$ 10d:

Orange solid (24.8 mg, 0.05 mmol, 84%); the characterization data are as follows and consistent with the reported data.[31] m.p. = 228 ~ 230 $^\circ\text{C}$; ^1H NMR (300 MHz, CDCl_3 , 298 K) δ (ppm): 7.49- 7.35 (m, 4H), 7.23-7.20 (m, 3H), 6.59 (d, $J = 7.9$ Hz, 1H), 3.91 (s, 3H), 2.39 (s, 3H), 1.42(s, 15H); HRMS (ESI) for $\text{C}_{25}\text{H}_{29}\text{ClIrNO}$ $[\text{M}-\text{Cl}]^+$: m/z calc.: 552.1878, Found: 552.1873.

$[(\eta^5\text{-Cp}^*)\text{Ir}(\text{E})\text{-N-(4-chlorophenyl)-1-(p-tolyl)ethan-1-imine)Cl]$ 10e:

Yellow solid (27.5 mg, 0.05 mmol, 91%); m.p. = 287 ~ 289 $^\circ\text{C}$; ^1H NMR (400 MHz, CDCl_3 , 298 K) δ (ppm): 7.98 – 7.70 (m, 1H), 7.64 (s, 1H), 7.41 (t, $J = 7.3$ Hz, 3H), 6.85 (dd, $J = 7.9, 1.1$ Hz, 2H), 2.45 (s, 3H), 2.42 (s, 3H), 1.43 (s, 15H); ^{13}C NMR (100 MHz, CDCl_3 , 298 K) δ (ppm): 181.53, 168.68, 149.31, 145.01, 142.50, 135.77, 131.58, 128.59, 122.73, 88.97, 53.40, 30.90, 21.98, 16.79, 8.52; IR (thin film, cm^{-1}): 2963, 2359, 1575, 1455, 1375, 1261, 1013, 802, and 749; HRMS (ESI) for $\text{C}_{25}\text{H}_{28}\text{Cl}_2\text{IrN}$ $[\text{M}-\text{Cl}]^+$: m/z calc.: 570.1540, Found: 570.1519.

$[(\eta^5\text{-Cp}^*)\text{Ir}(\text{E})\text{-N-phenyl-1-(p-tolyl)ethan-1-imine)Cl]$ 10f:

Orange solid (25.4 mg, 0.05 mmol, 89%); the characterization data are as follows and consistent with the reported data.[31] m.p. = 255 ~ 258 $^\circ\text{C}$; ^1H NMR (300 MHz, CDCl_3 , 298 K) δ (ppm): 7.64 (s, 1H), 7.41 (d, $J = 7.4$ Hz, 3H), 7.25-7.21 (m, 2H), 6.84 (d, $J = 7.2$ Hz, 2H), 2.45 (s, 3H), 2.41 (s, 3H), 1.41 (s, 15H); HRMS (ESI) for $\text{C}_{25}\text{H}_{29}\text{ClIrN}$ $[\text{M}-\text{Cl}]^+$: m/z calc.: 536.1929, Found: 536.1925.

$[(\eta^5\text{-Cp}^*)\text{Ir}(\text{E})\text{-N,1-di-p-tolyethan-1-imine)Cl}]$ 10g:

Yellow solid (27.2 mg, 0.05 mmol, 93%); m.p. = 238 ~ 240 °C; ^1H NMR (400 MHz, CDCl_3 , 298 K) δ (ppm): ^1H NMR (400 MHz, CDCl_3) δ 7.55 (s, 2H), 7.32 (d, $J = 7.9$ Hz, 1H), 7.13 (d, $J = 7.3$ Hz, 2H), 6.76 (dd, $J = 7.9, 1.1$ Hz, 2H), 2.37 (s, 3H), 2.32 (d, $J = 2.5$ Hz, 6H), 1.34 (s, 15H); ^{13}C NMR (100 MHz, CDCl_3 , 298 K) δ (ppm): 180.80, 168.11, 148.26, 145.33, 141.94, 135.63, 128.19, 122.45, 88.81, 21.89, 20.93, 16.68, 8.41; IR (thin film, cm^{-1}): 2961, 2367, 1574, 1451, 1375, 1261, 1019, 800, and 749; HRMS (ESI) for $\text{C}_{26}\text{H}_{31}\text{ClIrN}$ $[\text{M-Cl}]^+$: m/z calc.: 550.2086, Found: 550.2081.

 $[(\eta^5\text{-Cp}^*)\text{Ir}(\text{E})\text{-1-(4-nitrophenyl)-N-(p-tolyl)ethan-1-imine)Cl}]$ 10h:

Brown solid (27.7 mg, 0.05 mmol, 89%); m.p. = 275 ~ 277 °C; ^1H NMR (400 MHz, CDCl_3 , 298 K) δ (ppm): 8.61 (d, $J = 2.3$ Hz, 1H), 7.86 (dd, $J = 8.5, 2.3$ Hz, 1H), 7.76 – 7.67 (m, 1H), 7.61 (d, $J = 8.5$ Hz, 3H), 6.90 – 6.67 (m, 1H), 2.48 (s, 3H), 2.42 (s, 3H), 1.44 (s, 15H); ^{13}C NMR (100 MHz, CDCl_3 , 298 K) δ (ppm): 180.23, 168.65, 153.38, 148.97, 147.86, 136.68, 129.16, 128.48, 116.79, 90.03, 21.03, 17.43, 8.50; IR (thin film, cm^{-1}): 2961, 2357, 1504, 1446, 1332, 1260, 1019, 796, and 758; HRMS (ESI) for $\text{C}_{25}\text{H}_{28}\text{ClIrN}_2\text{O}_2$ $[\text{M-Cl}]^+$: m/z calc.: 581.1780, Found: 581.1812.

 $[(\eta^5\text{-Cp}^*)\text{Ir}(\text{E})\text{-1-phenyl-N-(p-tolyl)ethan-1-imine)Cl}]$ 10i:

Yellow solid (22.5 mg, 0.05 mmol, 78%); m.p. = 202 ~ 204 °C; ^1H NMR (400 MHz, CDCl_3 , 298 K) δ (ppm): 7.75 (d, $J = 7.6$ Hz, 1H), 7.63 (d, $J = 7.6$ Hz, 1H), 7.48 – 7.40 (m, 1H), 7.15 (dd, $J = 7.2, 6.2$ Hz, 3H), 6.94 (dd, $J = 11.0, 4.0$ Hz, 1H), 6.85 – 6.56 (m, 1H), 2.36 (s, 3H), 2.33 (s, 3H), 1.35 (s, 15H); ^{13}C NMR (100 MHz, CDCl_3 , 298 K) δ (ppm): 181.28, 168.14, 148.25, 147.75, 135.78, 135.03, 131.91, 128.36, 121.30, 89.02, 20.97, 16.79, 8.44; IR (thin film, cm^{-1}): 2982, 2364, 1579, 1448, 1374, 1261, 1025, 785, and 749; HRMS (ESI) for $\text{C}_{25}\text{H}_{29}\text{ClIrN}$ $[\text{M-Cl}]^+$: m/z calc.: 536.1929, Found: 536.1964.

 $[(\eta^5\text{-Cp}^*)\text{Ir}(\text{E})\text{-N-(4-chlorophenyl)-1-phenylethan-1-imine)Cl}]$ 10j:

Orange solid (25.1 mg, 0.05 mmol, 85%); m.p. = 271 ~ 273 °C; ^1H NMR (400 MHz, CDCl_3 , 298 K) δ (ppm): 7.76 (dd, $J = 7.6, 0.7$ Hz, 2H), 7.46 (dd, $J = 7.8, 1.1$ Hz, 1H), 7.34 (d, $J = 8.0$ Hz, 2H), 7.16 (dd, $J = 7.5, 1.3$ Hz, 1H), 6.97 (td, $J = 7.7, 1.1$ Hz, 1H), 6.77 (s, 1H), 2.38 (s, 3H), 1.37 (s, 15H); ^{13}C NMR (100 MHz, CDCl_3 , 298 K) δ (ppm): 182.03, 168.67, 149.26, 147.40, 135.14,

132.31, 131.74, 128.74, 121.53, 89.16, 30.91, 16.87, 8.53; IR (thin film, cm^{-1}): 2961, 2354, 1539, 1448, 1374, 1260, 1012, 797, and 749; HRMS (ESI) for $\text{C}_{24}\text{H}_{26}\text{Cl}_2\text{IrN}$ $[\text{M}-\text{Cl}]^+$: m/z calc.: 556.1383, Found: 556.1357.

$[(\eta^5\text{-Cp}^*)\text{Ir}(\text{E})\text{-1-(4-nitrophenyl)-N-phenylethan-1-imine)Cl]$ 10k:

Brown solid (25.9 mg, 0.05 mmol, 86%); m.p. = 275 ~ 277 °C; ^1H NMR (400 MHz, CDCl_3 , 298 K) δ (ppm): 8.62 (d, $J = 2.2$ Hz, 1H), 7.88 (d, $J = 2.3$ Hz, 1H), 7.86 (d, $J = 2.3$ Hz, 1H), 7.63 (d, $J = 8.5$ Hz, 1H), 7.48 (s, 2H), 7.29 (d, $J = 7.5$ Hz, 1H), 6.88 (s, 1H), 2.49 (s, 3H), 1.45 (s, 15H); ^{13}C NMR (100 MHz, CDCl_3 , 298 K) δ (ppm): 180.30, 168.78, 153.25, 150.24, 148.94, 129.12, 128.58, 126.91, 116.76, 90.05, 17.42, 9.32, 8.43; IR (thin film, cm^{-1}): 2961, 2367, 1510, 1448, 1378, 1258, 1011, 788, and 751; HRMS (ESI) for $\text{C}_{24}\text{H}_{26}\text{ClIrN}_2\text{O}_2$ $[\text{M}-\text{Cl}]^+$: m/z calc.: 567.1624, Found: 567.1662.

$[(\eta^5\text{-Cp}^*)\text{Ir}(\text{E})\text{-1-(4-chlorophenyl)-N-phenylethan-1-imine)Cl]$ 10l:

Yellow solid (22.7 mg, 0.05 mmol, 76%); m.p. = 231 ~ 233 °C; ^1H NMR (400 MHz, CDCl_3 , 298 K) δ (ppm): 7.77 (s, 1H), 7.68 (d, $J = 2.0$ Hz, 1H), 7.37 (d, $J = 8.2$ Hz, 2H), 7.16 (d, $J = 7.4$ Hz, 2H), 6.95 (dd, $J = 8.3, 2.0$ Hz, 1H), 6.80 (s, 1H), 2.35 (s, 3H), 1.35 (s, 15H); ^{13}C NMR (100 MHz, CDCl_3 , 298 K) δ (ppm): 180.55, 169.84, 150.51, 146.18, 137.84, 134.43, 129.55, 126.44, 121.64, 89.36, 17.04, 8.42; IR (thin film, cm^{-1}): 2961, 2371, 1530, 1448, 1373, 1259, 1014, 792, and 749; HRMS (ESI) for $\text{C}_{24}\text{H}_{26}\text{Cl}_2\text{IrN}$ $[\text{M}-\text{Cl}]^+$: m/z calc.: 556.1383, Found: 556.1403.

$[(\eta^5\text{-Cp}^*)\text{Ir}(\text{E})\text{-1-(2-chlorophenyl)-N-phenylethan-1-imine)Cl]$ 10m:

Yellow solid (23.3 mg, 0.05 mmol, 79%); m.p. = 232 ~ 234 °C; ^1H NMR (400 MHz, CDCl_3 , 298 K) δ (ppm): 7.80 (s, 1H), 7.64 (d, $J = 7.4$ Hz, 1H), 7.38 (d, $J = 32.7$ Hz, 2H), 7.15 (t, $J = 7.4$ Hz, 1H), 7.01 (t, $J = 7.6$ Hz, 1H), 6.94 (d, $J = 7.7$ Hz, 1H), 6.77 (s, 1H), 2.63 (s, 3H), 1.32 (s, 15H); ^{13}C NMR (100 MHz, CDCl_3 , 298 K) δ (ppm): 181.46, 171.91, 150.98, 143.34, 134.30, 132.39, 126.39, 124.74, 89.82, 23.13, 8.33; IR (thin film, cm^{-1}): 2962, 2362, 1557, 1449, 1377, 1260, 1023, 790, and 748; HRMS (ESI) for $\text{C}_{24}\text{H}_{26}\text{Cl}_2\text{IrN}$ $[\text{M}-\text{Cl}]^+$: m/z calc.: 556.1383, Found: 556.1413.

$[(\eta^5\text{-Cp}^*)\text{Ir}(\text{E})\text{-1-(4-fluorophenyl)-N-phenylethan-1-imine)Cl]$ 10n:

Yellow solid (25.6 mg, 0.05 mmol, 89%); m.p. = 202 ~ 204 °C; ^1H NMR (400 MHz, CDCl_3 , 298 K) δ (ppm): 7.84 (s, 1H), 7.52 (dd, $J = 8.5, 5.6$ Hz, 1H), 7.48 (dd, $J = 9.4, 2.5$ Hz, 1H), 7.44 (s, 2H), 7.23 (t, $J = 7.4$ Hz, 1H), 6.87 (s, 1H), 6.73 (td, $J = 8.7, 2.5$ Hz, 1H), 2.42 (s, 3H), 1.41 (s, 15H); ^{13}C NMR (100 MHz, CDCl_3 , 298 K) δ (ppm): 180.07, 171.35, 166.08, 163.54, 150.56, 144.06, 130.44, 126.32, 120.81, 108.74, 89.25, 17.08, 8.39; IR (thin film, cm^{-1}): 2960, 2369, 1544, 1448, 1373, 1259, 1014, 796, and 749; HRMS (ESI) for $\text{C}_{24}\text{H}_{26}\text{ClIrN}$ $[\text{M}-\text{Cl}]^+$: m/z calc.: 540.1679, Found: 540.1727.

$[(\eta^5\text{-Cp}^*)\text{Ir}(\text{E})\text{-1-(naphthalen-2-yl)-N-phenylethan-1-imine}]\text{Cl}$ 10o:

Yellow solid (21.9 mg, 0.05 mmol, 72%); the characterization data are as follows and consistent with the reported data.[30] m.p. = 247 ~ 249 °C; ^1H NMR (400 MHz, CDCl_3 , 253 K) δ (ppm): 8.17 (s, 1H), 8.08 (s, 1H), 7.91 (d, $J = 7.8$ Hz, 1H), 7.81 (dd, $J = 8.2, 2.8$ Hz, 2H), 7.57-7.41 (m, 3H), 7.35-7.29 (m, 2H), 6.93 (d, $J = 7.6$ Hz, 1H), 2.58 (s, 3H), 1.45 (s, 15H); HRMS for $\text{C}_{28}\text{H}_{29}\text{ClIrN}$ $[\text{M}]^+$: m/z calc.: 607.1605, Found: 607.1603.

3.2. Biological evaluation

3.2.1. Materials

Fetal bovine serum (FBS) was obtained from Hyclone (Thermo, South America). RPMI-1640 medium was obtained from Gibco BRL (NY, USA.). N-acetyl-L-cysteine (NAC), 3-(4, 5-dimethylthiazol-2-yl)-2, 5-diphenyl tetrazolium bromide (MTT), dimethyl sulfoxide (DMSO), 7'-dichlorodihydrofluorescein diacetate (DCFH-DA) were obtained from Sigma-Aldrich (St. Louis, USA.). Antibodies for cytochrome c (sc-13156), COX4I2 (sc-100522), Bcl-2 (sc-7382), Bax (sc-493), and β -Actin (sc-47778) were purchased from Santa Cruz Biotechnology (CA, USA). Secondary anti-mouse (BA1050), anti-rabbit (BA1054) antibodies were obtained from Boster Bio-Engineering Limited Company (Wuhan, China). The BCA protein kit, the Caspase-3 Activity Assay Kit, and the Caspase-9 Activity Assay Kit were products of the Beyontime Institute of Biotechnology (Shanghai, China). The enhanced chemiluminescence (ECL) detection Kit was obtained from Amersham Biosciences (Buckinghamshire, UK). Annexin V-FITC/PI Apoptosis Detection Kit was purchased from Key GEN Biological Engineering Materials Co. Ltd (Nanjing, China). Triton X-100, Bovine serum albumin (BSA), and 4', 6-diamidino-2-

phenylindole (DAPI) were purchased from Beijing Solarbio Science & Technology Co. Ltd (Beijing, China).

3.2.2. Cell culture and treatments

Human leukemia cell line K562 and its adriamycin-selected multidrug resistant subline K562/ADM were obtained from the Institute of Hematology, Chinese Academy of Medical Sciences (Tianjin, China). Human breast cancer cell line MCF-7, adriamycin-selected multidrug resistant subline MCF-7/ADM, and human non-small cell lung cancer cell line A549 were purchased from Keygen Biotech (Nanjing, China). All the cell lines were grown in RPMI 1640 medium containing 10% bovine serum (FBS) and 100 U antibiotics (benzylpenicillin sodium and gentamycin sulfate) at 37 °C in a humidified 5% CO₂ incubator. To maintain MDR phenotype, 1 mg/L adriamycin was added to K562/ADM and MCF-7/ADM cultures and maintained in the drug-free medium for at least two weeks before being used. Compounds were dissolved in DMSO with a stock concentration of 0.1 M for *in vitro* assays.

3.2.3. The MTT assay

Cells were cultured at a density of 1×10^5 /mL in a 96-well plate and allowed to attach overnight. After the incubation with the testing chemicals for 48 h, the cells were treated with the solution of MTT (5 mg/mL) at 37 °C for 4 h. The dark purple formazan crystals formed inside the intact mitochondria were solubilized with DMSO, and the absorbance was measured at 570 nm using a microplate reader (Multiskan Spectrum, Thermo Scientific). The inhibition rates were calculated on a plate-by-plate basis for the test wells. The IC₅₀ values were calculated based on the inhibitory rate curves using Bliss' method.

3.2.4. The ROS assay

K562 cells were seeded on 6-well plates. After incubation with the testing chemicals, cells from each group at a density of 1×10^6 were harvested and incubated with 10 μM DCFH-DA at 37 °C for 30 min in the dark. Cells were then washed with PBS, and the fluorescence intensity was measured in the channel at 515-545 nm (emission) for DCF (2',7'-dichlorofluorescein) with argon laser excitation at 488 nm using Flow Cytometry (BD FACSVerse). The intracellular DCF

intensity was also confirmed by inverted fluorescence microscopy (Leica DMI4000) at a magnification of 200-fold.

3.2.5. The analysis of mitochondrial membrane potential (MMP)

The membrane potential assay was based on the fluorescence intensity of JC-1 (a lipophilic and cationic dye). JC-1 emitted green fluorescence when the MMP was relatively low while JC-1 aggregates emitted red fluorescence when the mitochondrial membranes were disrupted. Briefly, K562 cells were treated with the testing chemicals respectively for 24 h and were incubated with 5 $\mu\text{g}/\text{mL}$ JC-1 at 37 $^{\circ}\text{C}$ for 20 min in the dark. The cells were rinsed twice with JC-1 staining buffer, and the fluorescence intensity was measured by flow cytometry (BD FACSVerse) and was observed using a confocal microscopy (Leica TCS SP8).

3.2.6. Measurements of cytochrome c

After the treatment with compound **10c** for 24 h, the cells were lysed in the preparation buffer (250 mM sucrose, 20 mM HEPES-KOH at pH of 7.4, 10 mM NaCl, 1.5 mM MgCl_2 , 1 mM EDTA, 1 mM EGTA, 1 mM dithiothreitol, 2 $\mu\text{g}/\text{mL}$ aprotinin, and 1 mM phenylmethylsulfonyl fluoride) for 10 min on ice followed by centrifugation at 10,000 rpm at 4 $^{\circ}\text{C}$ for 20 min to separate the cytosolic and mitochondrial fractions. Protein concentrations were measured using a BCA Protein Assay Kit (Beyotime). The contents of cytochrome c in the cytosol and mitochondria were determined by western blot.

3.2.7. Extraction, fractionation, and detection of cytosolic and mitochondrial cytochrome c

K562 cells ($2\text{-}5 \times 10^7$ per sample) were treated with the testing compounds for 24 h and harvested by centrifugation at $800 \times g$ for 5 min. The extraction and fractionation of cytosolic and mitochondrial cytochrome c were manipulated using mitochondria/cytosol isolation kit following the manufacturer's instructions (Applygen Technologies Inc. Beijing, China). Briefly, the pellets were washed once with ice-cold PBS, suspended with 1.5 ml pre-cold Mito-Cyto buffer in grinder, and then grinded about 20 times. The cellular homogenate was centrifuged at $800 \times g$ at 4 $^{\circ}\text{C}$ for 5 min to obtain the supernatants. The supernatants were then centrifuged at $12000 \times g$ at 4 $^{\circ}\text{C}$ for 10 min. The obtained supernatants were used for the identification of cytosolic cytochrome c and the pellets for mitochondrial cytochrome c were subjected to 15% SDS-PAGE

and immunoblotted. Cytochrome c oxidase IV was used as the loading control for the mitochondrial fraction.

3.2.8. Western blot

K562 cells from each group were treated with the testing compounds for 24 h and suspended in lysis buffer for 30 min with shaking at 4 °C. After centrifugation (10000×g) for 10 min, the supernatants were collected. Cell lysate (50 µg) was resolved on 4-12 % SDS-PAGE gels and then transferred onto the nitrocellulose membranes. The membranes were blocked with Tris-buffered saline with 0.1% Tween 20 and 5% skim milk, and were incubated with the primary antibodies overnight at 4 °C. The membranes were then washed with TBST for three times and incubated with HRP-conjugated secondary antibody at room temperature for 1 h. Following three-time wash with TBST, the membranes were developed by the ECL detection Kit. The images of the western blot were captured and analyzed by the Bio-rad imaging system.

3.2.9. Measurements of the caspase activity

The activities of caspase-3 and -9 were measured using the Caspase-3 Activity Assay Kit and the Caspase-9 Activity Assay Kit according to the kit manuals. K562 cells with or without treatments of compounds were lysed using 100 µL lysis buffer, and subsequently centrifuged at 16000 g at 4 °C for 10 min. The supernatant was collected. Next, 70 µL of the assay buffer was mixed with 20 µL of lysate in a 96-well plate, followed by the addition of 10 µL of 1 mM p-nitroaniline (pNA). The plate was then incubated at 37 °C in the dark for 1 h, and the relative fluorescence unit value for the emission at 405 nm was measured. The result was normalized to the total protein measured using the Bradford assay.

3.2.10. Determination of the apoptotic rate

The apoptotic rate of K562 cells was detected by the Annexin V-FITC/PI double labeling method. The cell suspension was centrifuged and re-suspended in 195 µL Annexin V-FITC binding buffer and incubated with 5 µL Annexin V-FITC in the dark at ambient temperature for 10 min. Cells were centrifuged, and the pellets were re-suspended in 195 µL binding buffer. Cells were then incubated with 10 µL PI solution on an ice bath in the dark for 10 min. The

suspension of each group was analyzed by flow cytometry (BD FACSVerge). The fluorescence of Annexin V-FITC and PI was also observed using a confocal microscopy (Leica TCS SP8).

3.2.11. The cell cycle assay

Following the incubation of the testing chemicals for 24 h, 1×10^6 cells were harvested and fixed in 70% cold ethanol at 4 °C for 12 h. Then, cells were washed twice with PBS, re-suspended in 150 μ L of 100 μ g/mL RNase solution (in 0.2 M citrate-phosphate buffer, pH 7.8), and incubated at 37 °C for 30 min. Finally, cells were stained with 100 μ g/mL PI solution at room temperature in the dark. The fluorescence activity of the remaining DNA content was analyzed by flow cytometry (BD FACSVerge).

3.2.12. Statistical analysis

All experiments were performed in triplicates. Significant differences among the groups were determined by one-way ANOVA analysis followed by Dunnett's multiple comparison tests. P-values less than 0.05 were considered as statistically significant.

4. Concluding Remarks

In conclusion, we synthesized a series of "half-sandwich" Schiff-base Ir(III) complexes and evaluated their activities against the K562 cell line. All compounds exhibited IC_{50} values of less than 5 μ M in K562 cells. The most potent compound **10c** in K562 cells ($IC_{50} = 0.26 \mu$ M) also displayed cytotoxicity against a panel of other cancer cell lines/sublines including K562/A02, MCF-7, MCF-7/ADM, and A549. Notably, compound **10c** outperformed cisplatin in all cells tested. The flow cytometric analysis with Annexin V-FITC/PI staining indicated that compound **10c** induced apoptosis of the cancer cells. Experiments also showed that compound **10c** increased the iROS level and decreased MMP. Further investigation illustrated that the treatment of **10c** led to upregulation of Bax and caspase-9, downregulation of Bcl-2, and release of cytochrome c in K562 cells, which suggested that compound **10c** induce apoptosis through the intrinsic mitochondria apoptosis pathway.

Acknowledgements

We appreciate the funding support from Sichuan University, the National Natural Science

Foundation of China (Grant no. U1204830), and the Science and Technology Key Project of Department of Education of Henan Province (Grants nos. 13A310064 and 15A360016).

ACCEPTED MANUSCRIPT

Figure 1. Representative Ir(III) complexes

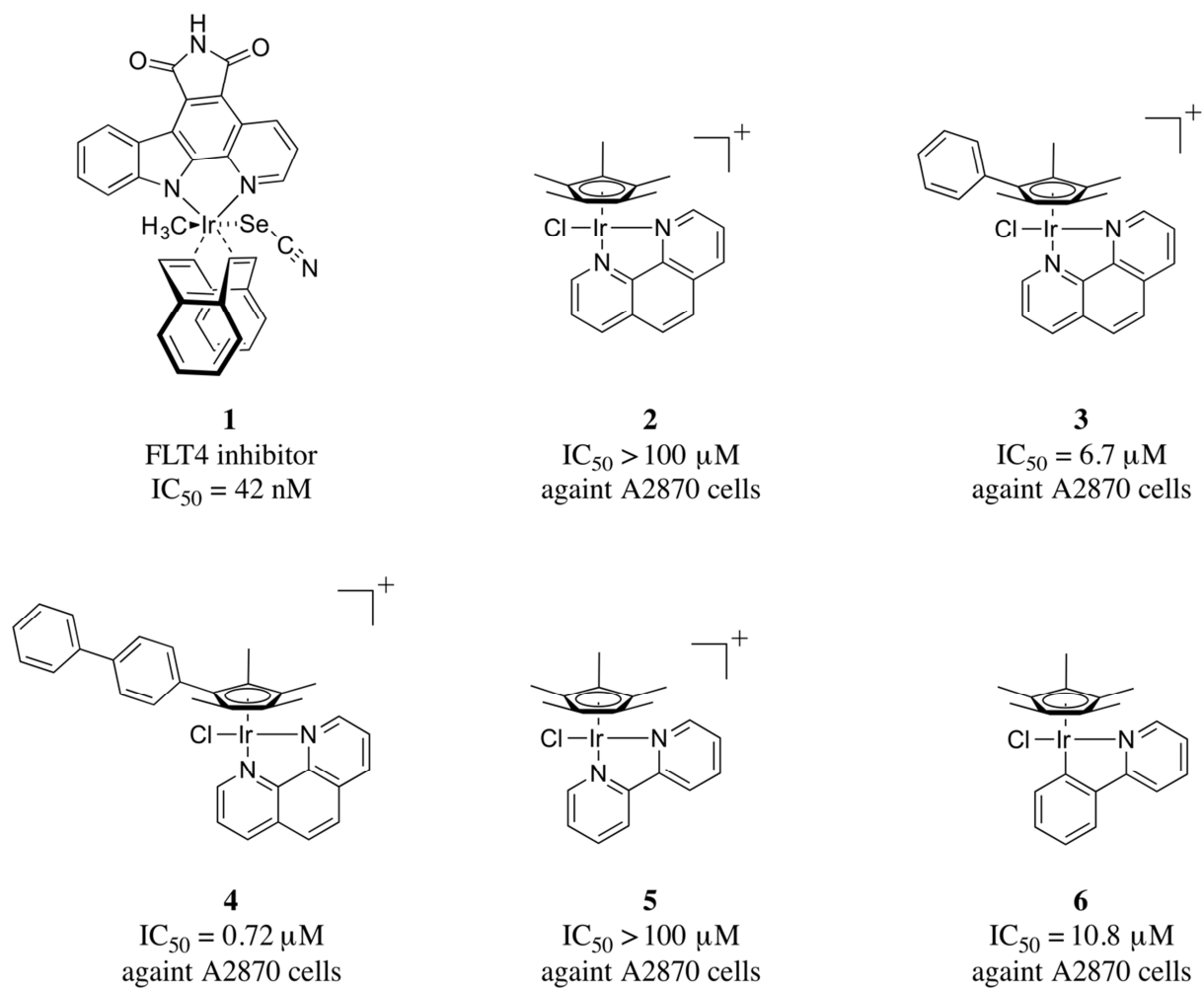


Figure 2. Compound **10c** increased the generation of reactive oxygen species (ROS). (A) Flow cytometric analysis of ROS generation. (B) Fluorescence microscopy analysis of ROS generation. Cells were treated with 1 μM compound **10c**, 1 μM compound **10c** + 2 mM NAC, and 5 μM cisplatin for 24 h, respectively, and then incubated with 10 μM DCFH-DA. Statistical data were shown as mean \pm SD (n =3). Significant differences relative to the control group were indicated as * for $P < 0.05$ and ** for $P < 0.01$; significant differences relative to the group with 1 μM compound **10c** were indicated as # for $P < 0.05$ and ## for $P < 0.01$.

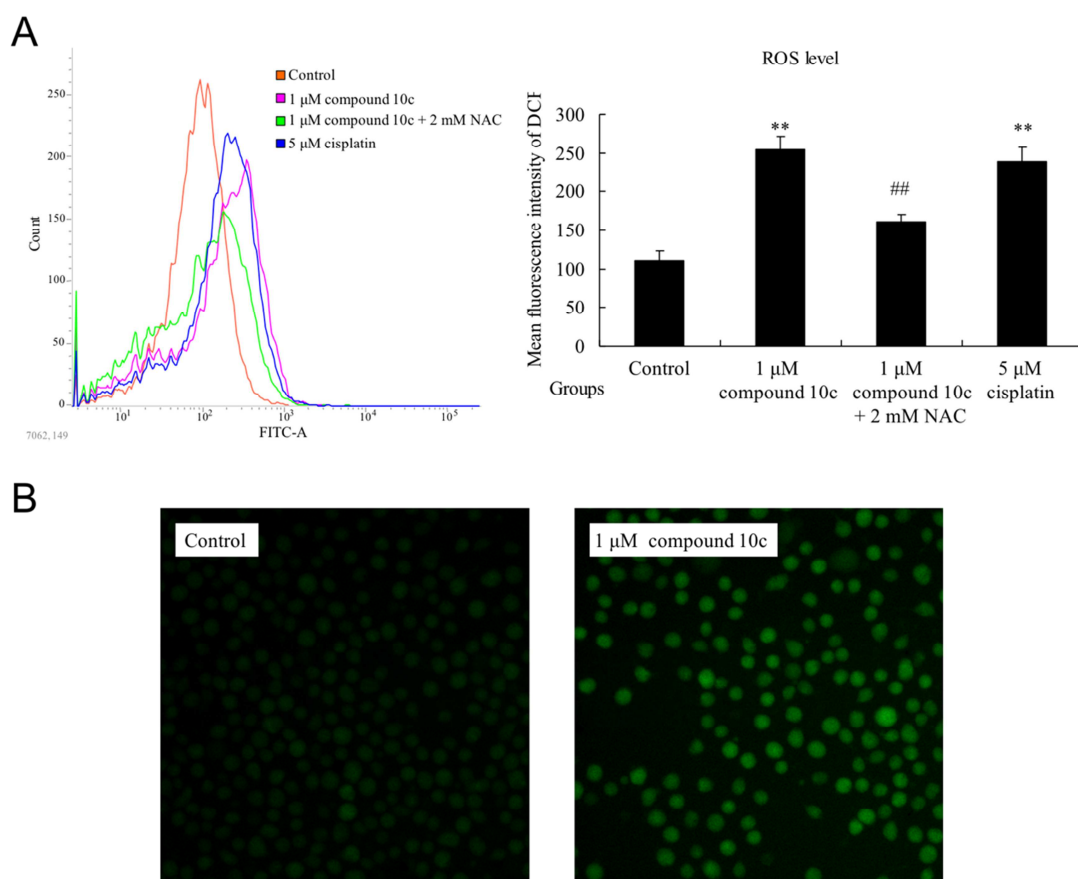


Figure 3. Apoptosis induction of compound **10c** in K562 cells were determined under light microscopy (200 \times), Flow Cytometry and Confocal Microscopy. K562 cells were incubated with 1 μ M compound **10c**, 1 μ M compound **10c** + 2 mM NAC, and 5 μ M cisplatin for 24 h, respectively, and then incubated with Annexin V-FITC (green) and PI (red). Shown are the representative results from three independent experiments.

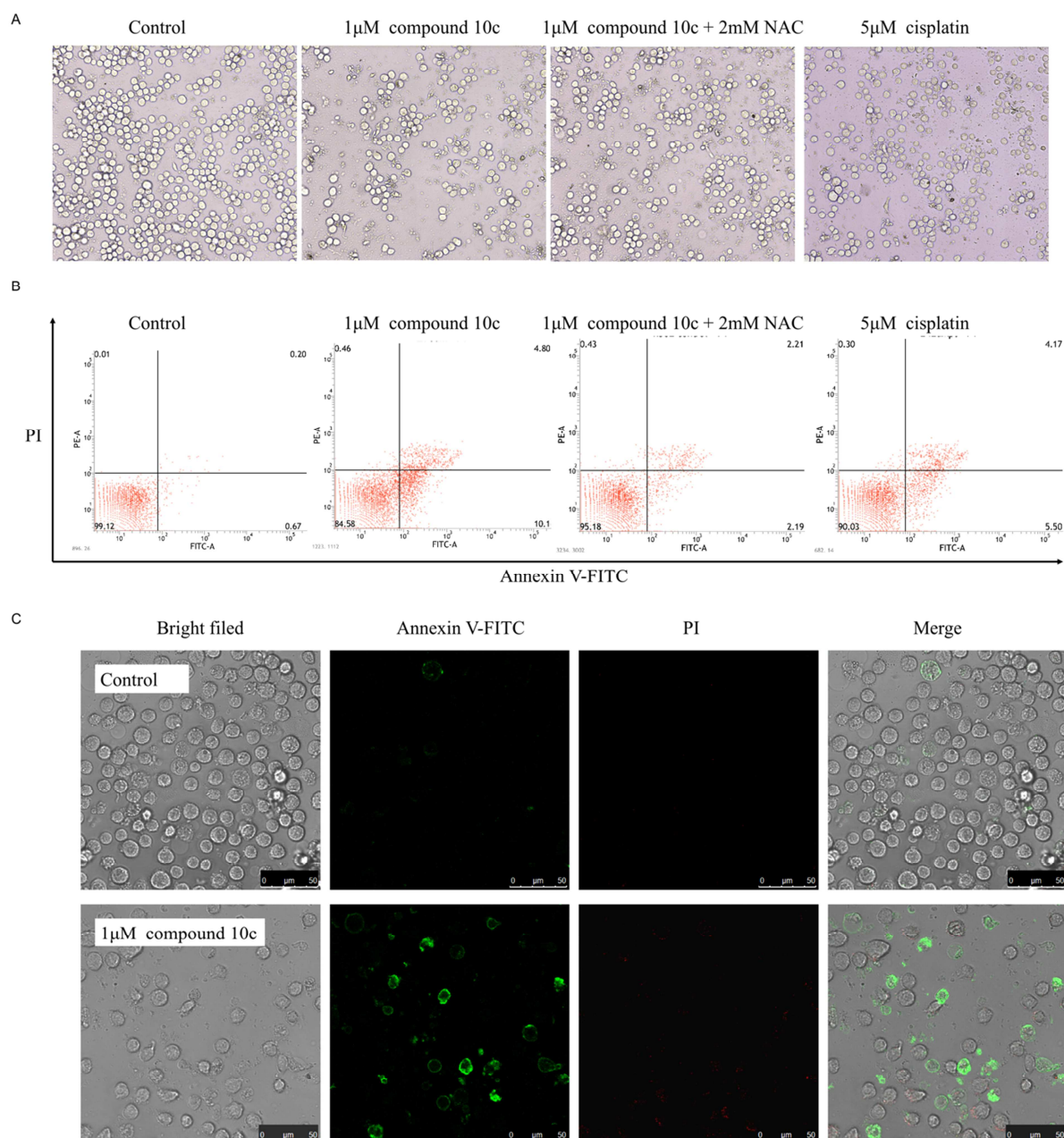


Figure 4. Compound **10c** induced depolarization of mitochondria membrane potential in K562 cells. (A) Flow cytometric analysis of the depolarization of the mitochondria membrane potential. (B) Confocal Microscopy analysis of the fluorescence of JC-1 aggregates (red) and JC-1 monomers (green). Cells were treated with 1 μ M compound **10c**, 1 μ M compound **10c** + 2 mM NAC, and 5 μ M cisplatin for 24 h, respectively, and then incubated with 5 μ g/mL JC-1. Shown are the representative results from three independent experiments.

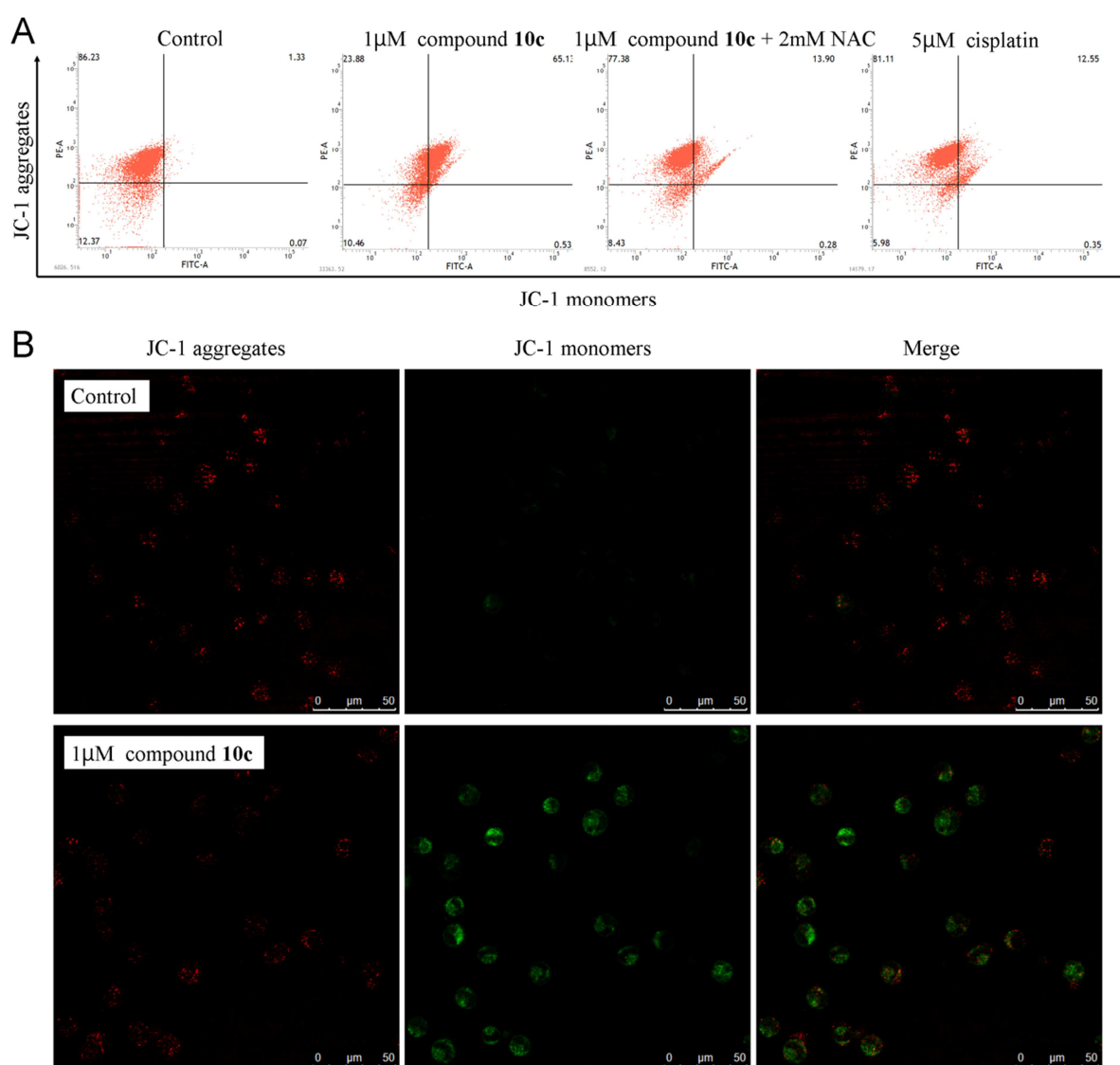


Figure 5. Compound **10c** activated the mitochondrial apoptotic pathway in K562 cells. (A) Concentration-dependent effects of compound **10c** on cytochrome c release from mitochondria to cytosol, and on the protein levels of Bcl-2 and Bax. The data were measured by western blot, and the representative images from three independent experiments were shown. (B) Activation of caspase-9 and caspase-3 induced by compound **10c**. Enzymatic activities of caspases were expressed as multiple proportions of the control. Statistical data were shown as mean \pm SD (n = 3). Significant differences relative to the control group were indicated as * for $P < 0.05$ and ** for $P < 0.01$.

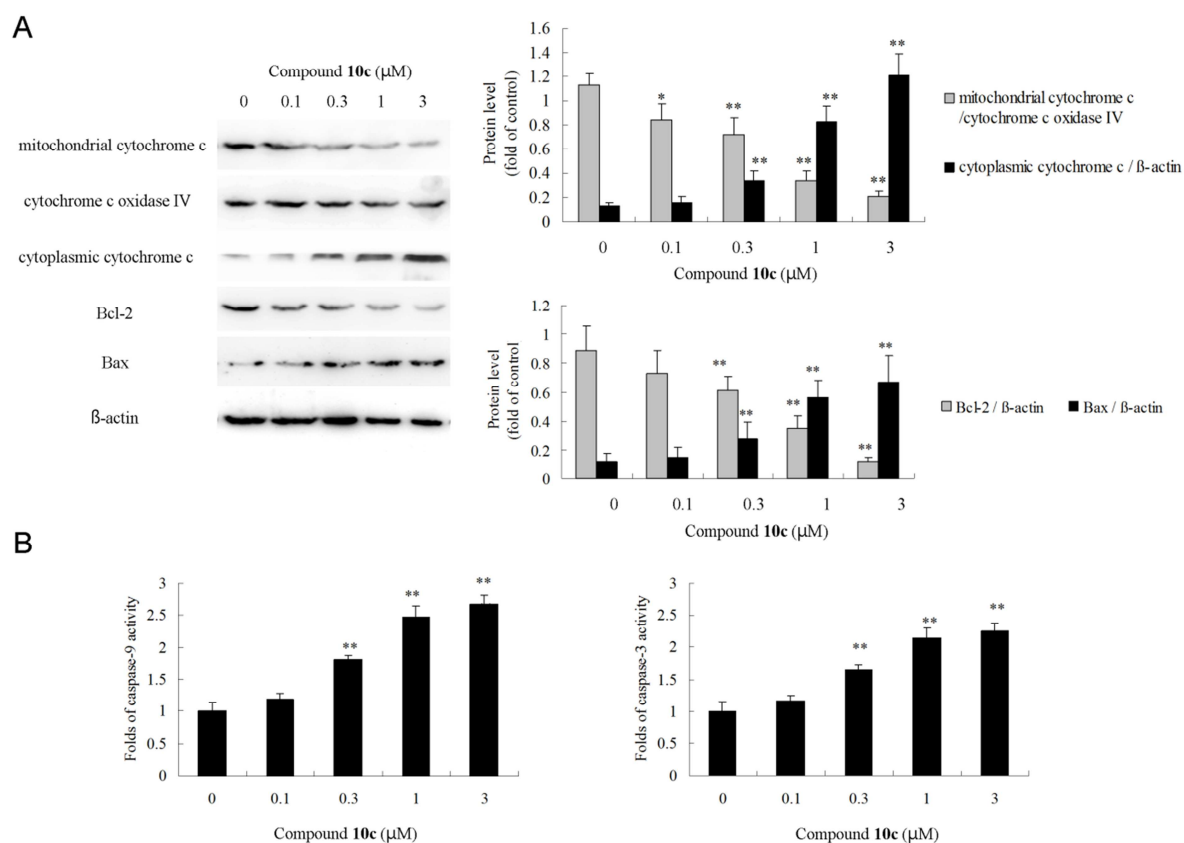
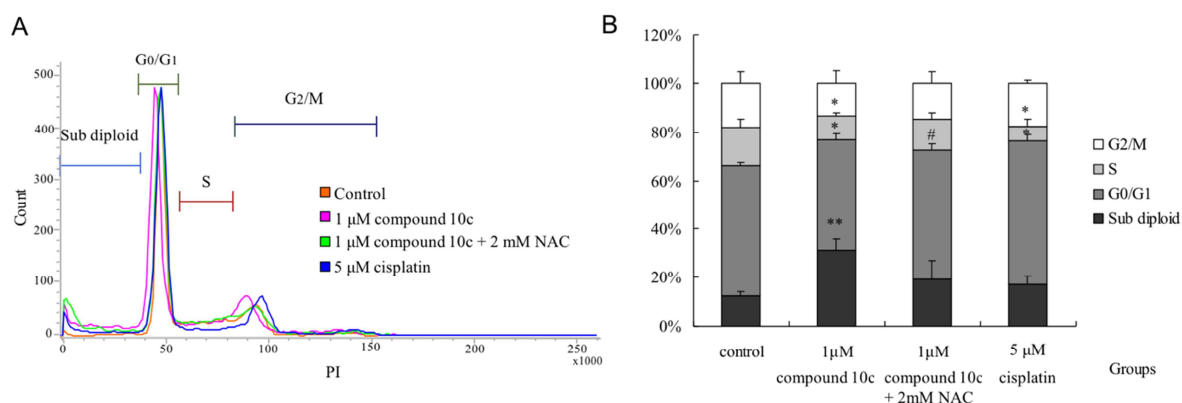
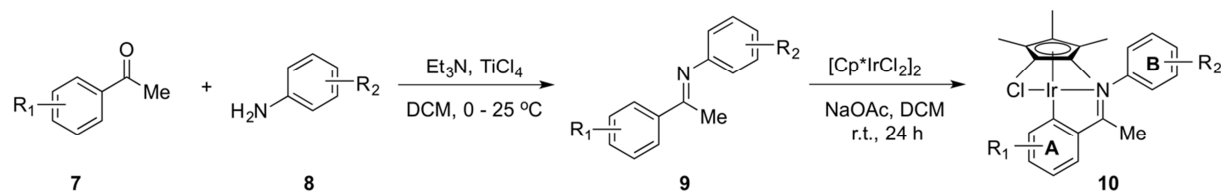


Figure 6. Effects of compound **10c** on the cell cycle of K562 cells treated for 48 h. Cells were incubated with 1 μ M compound **10c**, 1 μ M compound **10c** + 2 mM NAC, and 5 μ M cisplatin. Cell cycle distributions of the control cells and the chemical-treated cells were determined by propidium iodide (PI) staining and flow cytometric analysis. (A) Representative results from three independent experiments. (B) Statistical data were shown as mean \pm SD (n =3). Significant differences relative to the control group were indicated as * for $P < 0.05$ and ** for $P < 0.01$; significant differences relative to the group with 1 μ M compound **10c** were indicated as # for $P < 0.05$ and ## for $P < 0.01$.



Scheme 1. Synthetic route to Ir(III) complexes **10a-o** and their *in vitro* antiproliferative activities against K562 cells.



Entry	Compounds	R_1	R_2	IC_{50} (μM) ^{a,b}
1	10a	4-OMe	4-CN	1.10
2	10b	4-OMe	4-CF ₃	0.73
3	10c	4-OMe	4-OMe	0.26
4	10d	4-OMe	H	0.95
5	10e	4-Me	4-Cl	0.67
6	10f	4-Me	H	1.06
7	10g	4-Me	4-Me	0.53
8	10h	4-NO ₂	4-Me	1.00
9	10i	H	4-Me	0.62
10	10j	H	4-Cl	0.94
11	10k	4-NO ₂	H	4.77
12	10l	4-Cl	H	1.13
13	10m	2-Cl	H	0.61
14	10n	4-F	H	1.20
15	10o			0.87

^aValues were the average of three determinations.

^bThe IC_{50} of cisplatin against K562 is $5.86\text{ }\mu\text{M}$.

Table 1. Antiproliferative activities of compound **10c** against K562/A02, MCF-7, MCF-7/ADM, and A549 cells *in vitro*.

Compounds	IC ₅₀ (μM) ^a			
	K562/A02	MCF-7	MCF-7/ADM	A549
10c	1.95	5.52	18.81	2.09
cisplatin	6.56	7.46	36.52	16.03

^aValues were the average of three determinations.

References

- [1] I. Romero-Canelon, P.J. Sadler, Next-generation metal anticancer complexes: multitargeting via redox modulation, *Inorg Chem*, 52 (2013) 12276-12291.
- [2] P.C. Bruijninx, P.J. Sadler, New trends for metal complexes with anticancer activity, *Curr Opin Chem Biol*, 12 (2008) 197-206.
- [3] R. Cao, J. Jia, X. Ma, M. Zhou, H. Fei, Membrane localized iridium(III) complex induces endoplasmic reticulum stress and mitochondria-mediated apoptosis in human cancer cells, *J Med Chem*, 56 (2013) 3636-3644.
- [4] D. Wang, S.J. Lippard, Cellular processing of platinum anticancer drugs, *Nat Rev Drug Discov*, 4 (2005) 307-320.
- [5] T.C. Johnstone, K. Suntharalingam, S.J. Lippard, The Next Generation of Platinum Drugs: Targeted Pt(II) Agents, Nanoparticle Delivery, and Pt(IV) Prodrugs, *Chem Rev*, 116 (2016) 3436-3486.
- [6] L. Kelland, The resurgence of platinum-based cancer chemotherapy, *Nat Rev Cancer*, 7 (2007) 573-584.
- [7] L. Galluzzi, L. Senovilla, I. Vitale, J. Michels, I. Martins, O. Kepp, M. Castedo, G. Kroemer, Molecular mechanisms of cisplatin resistance, *Oncogene*, 31 (2012) 1869-1883.
- [8] Z. Liu, P.J. Sadler, Organoiridium complexes: anticancer agents and catalysts, *Acc Chem Res*, 47 (2014) 1174-1185.
- [9] A. Leonidova, G. Gasser, Underestimated potential of organometallic rhenium complexes as anticancer agents, *ACS Chem Biol*, 9 (2014) 2180-2193.
- [10] N. Muhammad, Z. Guo, Metal-based anticancer chemotherapeutic agents, *Curr Opin Chem Biol*, 19 (2014) 144-153.
- [11] D.L. Ma, D.S. Chan, C.H. Leung, Group 9 organometallic compounds for therapeutic and bioanalytical applications, *Acc Chem Res*, 47 (2014) 3614-3631.
- [12] Y. Geldmacher, M. Oleszak, W.S. Sheldrick, Rhodium(III) and iridium(III) complexes as anticancer agents, *Inorg Chim Acta*, 393 (2012) 84-102.
- [13] N. Graf, S.J. Lippard, Redox activation of metal-based prodrugs as a strategy for drug delivery, *Adv Drug Deliver Rev*, 64 (2012) 993-1004.
- [14] Z. Liu, A. Habtemariam, A.M. Pizarro, S.A. Fletcher, A. Kisova, O. Vrana, L. Salassa, P.C. Bruijninx, G.J. Clarkson, V. Brabec, P.J. Sadler, Organometallic half-sandwich iridium anticancer complexes, *J Med Chem*, 54 (2011) 3011-3026.
- [15] A. Cusanelli, U. Frey, D.T. Richens, A.E. Merbach, The slowest water exchange at a homoleptic mononuclear metal center: Variable-temperature and variable-pressure O-17 NMR study on $[\text{Ir}(\text{H}_2\text{O})_6]^{3+}$, *J Am Chem Soc*, 118 (1996) 5265-5271.
- [16] L. Messori, G. Marcon, P. Orioli, M. Fontani, P. Zanella, A. Bergamo, G. Sava, P. Mura, Molecular structure, solution chemistry and biological properties of the novel $[\text{ImH}][\text{trans} - \text{IrCl}_4(\text{Im})(\text{DMSO})]$, (I) and of the orange form of $[(\text{DMSO})_2\text{H}][\text{trans} - \text{IrCl}_4(\text{DMSO})_2]$, (II), complexes, *J Inorg Biochem*, 95 (2003) 37-46.
- [17] A. Kastl, A. Wilbuer, A.L. Merkel, L. Feng, P. Di Fazio, M. Ocker, E. Meggers, Dual anticancer activity in a single compound: visible-light-induced apoptosis by an antiangiogenic iridium complex, *Chem Commun*, 48 (2012) 1863-1865.
- [18] L. Feng, Y. Geisselbrecht, S. Blanck, A. Wilbuer, G.E. Atilla-Gokcumen, P. Filippakopoulos, K. Kraling, M.A. Celik, K. Harms, J. Maksimoska, R. Marmorstein, G.

- Frenking, S. Knapp, L.O. Essen, E. Meggers, Structurally sophisticated octahedral metal complexes as highly selective protein kinase inhibitors, *J Am Chem Soc*, 133 (2011) 5976-5986.
- [19] S. Schafer, W.S. Sheldrick, Coligand tuning of the DNA binding properties of half-sandwich organometallic intercalators: Influence of polypyridyl (pp) and monodentate ligands (L = Cl, (NH₂)₂CS, (NMe₂)₂CS) on the intercalation of (eta⁵-pentamethylcyclopentadienyl)iridium(III)-dipyridoquinoxaline and -dipyridophenazine complexes, *J Organomet Chem*, 692 (2007) 1300-1309.
- [20] Z. Liu, L. Salassa, A. Habtemariam, A.M. Pizarro, G.J. Clarkson, P.J. Sadler, Contrasting reactivity and cancer cell cytotoxicity of isoelectronic organometallic iridium(III) complexes, *Inorg Chem*, 50 (2011) 5777-5783.
- [21] S.C. Hockey, G.J. Barbante, P.S. Francis, J.M. Altimari, P. Yoganantharajah, Y. Gibert, L.C. Henderson, A comparison of novel organoiridium(III) complexes and their ligands as a potential treatment for prostate cancer, *Eur J Med Chem*, 109 (2016) 305-313.
- [22] T.S. Kang, Z. Mao, C.T. Ng, M. Wang, W. Wang, C. Wang, S.M. Lee, Y. Wang, C.H. Leung, D.L. Ma, Identification of an Iridium(III)-Based Inhibitor of Tumor Necrosis Factor- α , *J Med Chem*, 59 (2016) 4026-4031.
- [23] H.J. Zhong, L.H. Lu, K.H. Leung, C.C.L. Wong, C. Peng, S.C. Yan, D.L. Ma, Z.W. Cai, H.M.D. Wang, C.H. Leung, An iridium(III)-based irreversible protein-protein interaction inhibitor of BRD4 as a potent anticancer agent, *Chem Sci*, 6 (2015) 5400-5408.
- [24] R.R. Ye, C.P. Tan, L.N. Ji, Z.W. Mao, Coumarin-appended phosphorescent cyclometalated iridium(III) complexes as mitochondria-targeted theranostic anticancer agents, *Dalton T*, 45 (2016) 13042-13051.
- [25] R. Cao, J.L. Jia, X.C. Ma, M. Zhou, H. Fei, Membrane Localized Iridium(III) Complex Induces Endoplasmic Reticulum Stress and Mitochondria-Mediated Apoptosis in Human Cancer Cells, *J Med Chem*, 56 (2013) 3636-3644.
- [26] J. Liu, C.G. Cao, H.B. Sun, X. Zhang, D.W. Niu, Catalytic Asymmetric Umpolung Allylation of Imines, *J Am Chem Soc*, 138 (2016) 13103-13106.
- [27] M. Zhan, R.Z. Li, Z.D. Mou, C.G. Cao, J. Liu, Y.W. Chen, D.W. Niu, Silver-Assisted, Iridium-Catalyzed Allylation of Bis[(pinacolato)boryl]methane Allows the Synthesis of Enantioenriched Homoallylic Organoboronic Esters, *Acs Catal*, 6 (2016) 3381-3386.
- [28] C. Wang, H.Y. Chen, J. Bacsá, C.R. Catlow, J. Xiao, Synthesis and X-ray structures of cyclometalated iridium complexes including the hydrides, *Dalton Trans*, 42 (2013) 935-940.
- [29] Q. Zou, C. Wang, J. Smith, D. Xue, J. Xiao, Alkylation of Amines with Alcohols and Amines by a Single Catalyst under Mild Conditions, *Chem-Eur J*, 21 (2015) 9656-9661.
- [30] D. Talwar, N.P. Salguero, C.M. Robertson, J.L. Xiao, Primary Amines by Transfer Hydrogenative Reductive Amination of Ketones by Using Cyclometalated Ir-III Catalysts, *Chem-Eur J*, 20 (2014) 245-252.
- [31] Y.W. Wei, D. Xue, Q. Lei, C. Wang, J.L. Xiao, Cyclometalated iridium complexes for transfer hydrogenation of carbonyl groups in water, *Green Chem*, 15 (2013) 629-634.

Highlights:

1. Fifteen “half-sandwich” Schiff-base Ir(III) complexes were investigated.
2. Compound **10c** displayed cytotoxicity against five cancer cell lines/sublines.
3. **10c** increased ROS level and decreased the mitochondrial membrane potential of K562 cells.
4. **10c** induced the apoptosis of K562 cells.